Proximity Effect between Two Superconductors Spatially Resolved by Scanning Tunneling Spectroscopy

V. Cherkez,[1,2] J. C. Cuevas,[3,*] C. Brun,[1,2,†] T. Cren,[1,2] G. Ménard,[1,2] F. Debontridder,[1,2] V. S. Stolyarov,[1,2,5,6] and D. Roditchev[1,4]

[1]*Institut des Nanosciences de Paris, Sorbonne Universités, UPMC Université Paris 06, UMR 7588, F-75005 Paris, France*

[2]*CNRS, UMR 7588, Institut des Nanosciences de Paris, F-75005 Paris, France*

[3]*Departamento de Física Teórica de la Materia Condensada and Condensed Matter Physics Center (IFIMAC), Universidad Autónoma de Madrid, E-28049 Madrid, Spain*

[4]*LPEM, ESPCI ParisTech-UPMC, CNRS-UMR 8213, 10 rue Vauquelin, 75005 Paris, France*

[5]*Moscow Institute of Physics and Technology, 141700 Dolgoprudny, Russia*

[6]*Institute of Solid State Physics, Russian Academy of Sciences, 142432 Chernogolovka, Russia*

(Received 2 January 2014; revised manuscript received 23 January 2014; published 11 March 2014)

We present a combined experimental and theoretical study of the proximity effect in an atomic-scale controlled junction between two different superconductors. Elaborated on a Si(111) surface, the junction comprises a Pb nanocrystal with an energy gap $\Delta_1 = 1.2$ meV, connected to a crystalline atomic monolayer of lead with $\Delta_2 = 0.23$ meV. Using *in situ* scanning tunneling spectroscopy, we probe the local density of states of this hybrid system both in space and in energy, at temperatures below and above the critical temperature of the superconducting monolayer. Direct and inverse proximity effects are revealed with high resolution. Our observations are precisely explained with the help of a self-consistent solution of the Usadel equations. In particular, our results demonstrate that in the vicinity of the Pb islands, the Pb monolayer locally develops a finite proximity-induced superconducting order parameter, well above its own bulk critical temperature. This leads to a giant proximity effect where the superconducting correlations penetrate inside the monolayer a distance much larger than in a nonsuperconducting metal.

DOI: 10.1103/PhysRevX.4.011033

Subject Areas: Condensed Matter Physics, Superconductivity

I. INTRODUCTION

If a normal metal (N) is in good electrical contact with a superconductor (S), Cooper pairs can leak from S to N, modifying the properties of the metal. This phenomenon, known as a proximity effect, was intensively studied in the 1960s [1,2], and there has been a renewed interest in the last two decades because of the possibility of studying this effect at much smaller length and energy scales [3]. When a Cooper pair penetrates into a normal metal, via an Andreev reflection [4], it becomes a pair of time-reversed electron states that propagate coherently over a distance L_C, which in diffusive metals is given by $L_C = \min\{\sqrt{\hbar D/E}, L_\phi\}$, where D is the diffusion constant, E is the energy of the electron states (with respect to the Fermi energy), and L_ϕ is the phase-coherence length in N. This Cooper pair leakage modifies the local density of states (DOS) of the normal metal over a distance L_C from the S-N interface. Such a modification has been spatially resolved in recent years with the help of tunneling probes [5,6] and with scanning tunneling microscopy/spectroscopy (STM/STS) techniques applied to mesoscopic systems [7–11]. Very recently, the considerable progress in the controlled growth of atomically clean materials under ultrahigh vacuum conditions has made it possible to probe the proximity effect with high spatial and energy resolution in *in situ* STM/STS experiments [12,13].

The proximity effect is not exclusive of S-N systems. If a superconductor S_1, with a critical temperature T_{C1} and energy gap Δ_1, is brought into contact with another superconductor S_2 with a lower critical temperature $T_{C2} < T_{C1}$ and energy gap $\Delta_2 < \Delta_1$, the local DOS of both superconductors near the interface is expected to be modified. At low enough temperature, $T < T_{C2}$, this modification should be significant in the energy interval $|E| \in [\Delta_1, \Delta_2]$ and may occur in each electrode over a distance $\min\{\sqrt{\hbar D/\Delta_i}, L_{\phi_i}\}$ from the interface. Moreover, in the temperature range $T_{C2} < T < T_{C1}$, one expects the proximity effect to induce a finite local order parameter in a formally nonsuperconducting S_2, owing to a nonzero attractive pairing interaction λ_2 existing in S_2. Such a

*juancarlos.cuevas@uam.es

†christophe.brun@insp.upmc.fr

mechanism should result in a proximity-induced interface superconductivity. These remarkable effects were first discussed qualitatively by de Gennes and co-workers in the 1960s [1,2], but to the best of our knowledge, no experiment has ever been reported in which this peculiar S_1-S_2 proximity effect could be spatially resolved.

In this work, we present a STM/STS study of the proximity effect in a lateral S_1-S_2 junction with a very high spatial and energy resolution, for temperatures well below and above T_{C2}. The junction was elaborated *in situ* in ultrahigh vacuum on Si(111). The S_1 electrode is formed by a single nanocrystal of Pb ($T_{C1} \approx 6.2$ K, $\Delta_1 = 1.2$ meV). S_2 consists of a single atomic layer of Pb reconstructed on Si(111) to form the so-called striped incommensurate phase, a superconductor with $T_{C2} \approx 1.8$ K and $\Delta_2 = 0.23$ meV. For temperatures well below T_{C2}, we observe a pronounced modification of the local tunneling conductance spectra in S_2 over a distance of around 100 nm from the S_1-S_2 interface. Above T_{C2} but below T_{C1}, the tunneling spectra in S_2 exhibit an induced gap that extends to distances anomalously large for a normal metal. Our experimental observations are explained with the help of a one-dimensional model based on the Usadel equations, where the order parameter is evaluated self-consistently. Importantly, our combined experimental and theoretical study furnishes strong evidence that the long-range proximity effect observed in S_2 above T_{C2} is a direct consequence of the appearance of proximity-induced interface superconductivity in the atomic monolayer (ML).

The paper is organized as follows. Section II describes the fabrication of the atomic-scale controlled junctions between two different superconductors and presents the results for the tunneling spectra in the low-temperature regime where both electrodes are in the superconducting state. Section III is devoted to the discussion of the theoretical model based on the Usadel theory that is used to describe all our experimental results. In Sec. IV, we present and discuss the results for the tunneling spectra in the temperature regime where the Pb monolayer is in its normal state. Then, we briefly discuss the inverse proximity effect in the Pb islands and summarize our main conclusions in Sec. V.

II. PROXIMITY EFFECT BETWEEN TWO SUPERCONDUCTORS: EXPERIMENTAL SETUP AND LOW-TEMPERATURE RESULTS

The fabrication of an S_1–S_2 junction was carried out *in situ* as we proceed to explain. First, a 7×7 reconstructed *n*-Si(111) surface (heavily doped) was prepared by direct-current heating at 1200°C in ultrahigh vacuum. Subsequently, a 1.65 monolayer of Pb was evaporated on the Si(111)-7×7 kept at room temperature, using an electron-beam evaporator calibrated with a quartz microbalance. The $\sqrt{7} \times \sqrt{3}$ reconstructed Pb monolayer was formed by annealing at 230°C for 30 minutes [14]. The slightly denser striped incommensurate phase was then formed by adding 0.2 ML of Pb onto the $\sqrt{7} \times \sqrt{3}$-Pb/Si (111) held at room temperature [15,16]. This resulted in a slightly extra amount of lead atoms (0.07 ML) with respect to the nominal reported coverage of the striped incommensurate phase (1.33 ML).

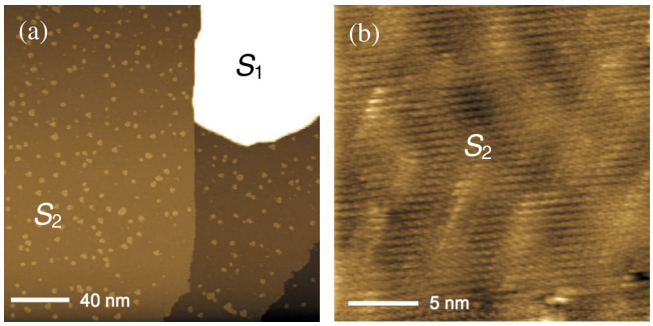

FIG. 1. (a) Topographical STM image of a 7-ML-high Pb island, denoted as S_1, surrounded by the SIC Pb monolayer, denoted as S_2. Small Pb clusters of few-nanometers size and 1-ML height are visible on the SIC monolayer. These very small clusters result from the extra Pb atoms deposited on the surface in order to form few large islands such as S_1. (b) Topographical STM image showing a smaller-scale region representing the atomic superstructure of the SIC monolayer observed everywhere on the surface between the Pb clusters. The images were taken at $V_{\text{bias}} = -1.0$ V and $I = 35$ pA.

This procedure allowed us to grow a very small density of Pb islands of size larger than 100 nm and height of 7 ML, such as the one denoted by S_1 in the STM topographic image shown in Fig. 1(a). These islands have a critical temperature and an energy gap slightly smaller than the bulk Pb values—here, $T_{C1} \approx 6.2$ K and $\Delta_1 \approx 1.2$ meV [17–20]. The island S_1 shown in Fig. 1(a) is in direct electrical contact through peripheral atoms with the striped incommensurate (SIC) monolayer denoted S_2, reported to be a superconductor with $T_{C2} \approx 1.8$ K and $\Delta_2 \approx 0.3$ meV [21,22]. It has been shown by various surface techniques that the Pb islands lay directly on top of the Si(111)-7×7 substrate [23]. In addition, one can see in Fig. 1(a) the formation of very tiny 1-ML-high nanoprotrusions or clusters on top of the striped incommensurate phase (less than 5 nm), also resulting from the deposition of the extra 0.07 ML of Pb. As presented in Fig. 1(b), the atomic superstructure of the SIC was observed everywhere on the surface between the overlying Pb islands or clusters. At each step, the sample structure was controlled in both real and reciprocal space by STM and low energy electron diffraction. The STS measurements were performed *in situ* with a homemade apparatus, at a base temperature of 320 mK and in ultrahigh vacuum $P < 4.0\ 10^{-11}$ mbar [19,24]. Mechanically sharpened Pt-Ir tips were used. The tunneling conductance curves $dI(V)/dV$ were obtained from numerical derivatives of the raw $I(V)$ experimental data.

Let us first discuss the results obtained at low temperature, $T = 0.3$ K $< T_{C1}, T_{C2}$, when both electrodes are in

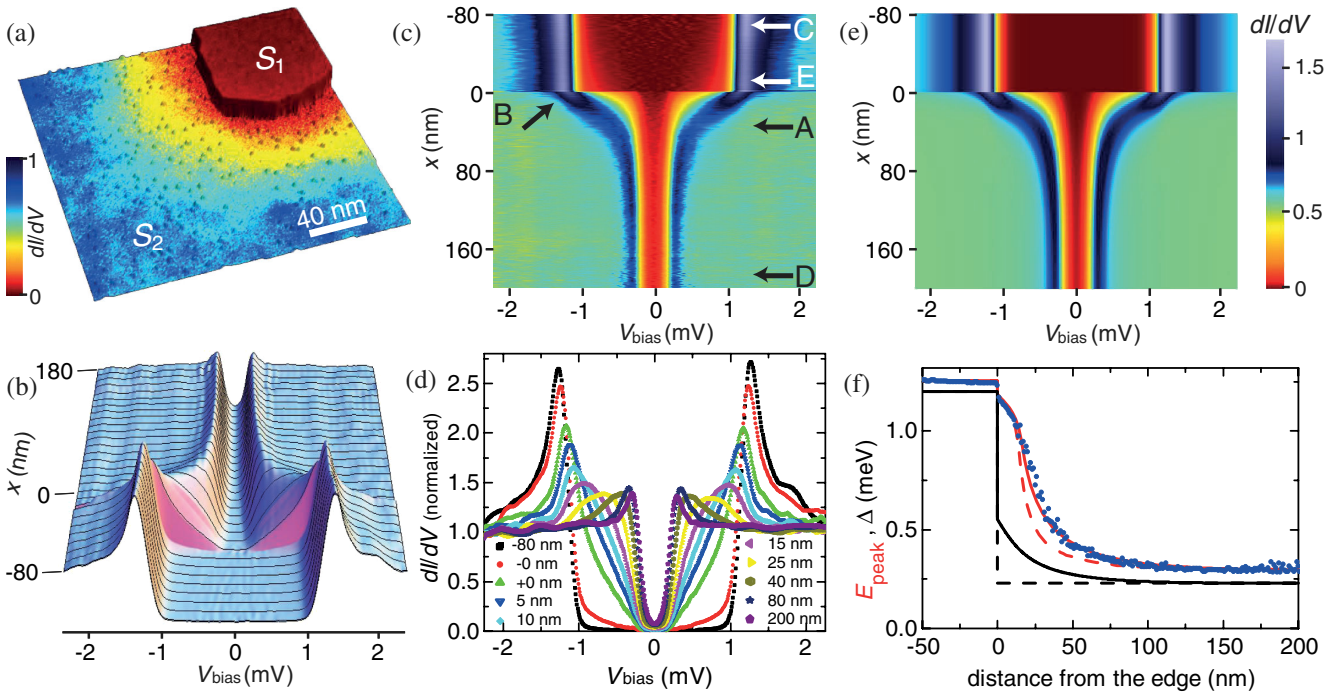

FIG. 2. S_1-S_2 proximity effect at 0.3 K. (a) Topographic STM image of the sample showing the Pb nanoisland S_1 connected to the striped incommensurate Pb monolayer S_2. The superposed color-coded spectroscopy map at $V_{bias} = -0.2$ mV allows one to visualize the proximity effect. The 256×256 spectra were measured in the STS map. (b) Spatial and energy evolution of the experimental tunneling conductance spectra, $dI/dV(V,x)$, across the junction (3 D view). One spectrum is plotted every 1 nm and highlighted by a black line every 10 nm. (c) Color-coded experimental $dI/dV(V,x)$ spectra across the interface. One spectrum is plotted every nanometer. (d) Selected local tunneling spectra (dots). The last spectrum measured on the top flat part of the island before the edge is denoted by -0 nm. The first spectrum measured on the SIC monolayer is denoted by $+0$ nm. The distance between the $+0$-nm and -0-nm spectra is about 1 nm. (e) Color-coded computed $dI/dV(V,x)$ across the interface. (f) Spatial evolution of the energy of the peak maximum $E_{peak}(x)$ across the interface. The experimental results (symbols) are nicely reproduced by self-consistent calculation of the order parameter (red solid line), while the red dashed line corresponds to the non-self-consistent result. The evolution of the order parameter is shown by black lines: self-consistent (solid) and non-self-consistent (dashed).

the superconducting state. These results are summarized in Fig. 2. In particular, panel (a) displays the S_1-S_2 junction considered throughout this work, where S_1 is the Pb island and S_2 corresponds to the SIC monolayer. The color-coded conductance map shown in this panel, at a bias voltage close to the S_2 gap edge, emphasizes that the proximity effect extends significantly far from the island edge. Let us stress that in Figs. 2, 3, and 5, one single $dI/dV(V,x)$ spectrum corresponds to the average of all $dI/dV(V,x)$ spectra measured at the same distance x from the island edge (the S_1-S_2 interface) in Fig. 1(a). As can be seen from the extension of the superconducting correlations shown in Figs. 2(a) and 3(a), this averaging procedure represents the main behavior well when going away from all island edges except in the vicinity of the sharp corner region, where the extension of the superconducting correlation is slightly reduced. Figures 2(b) and 2(c) show the detailed evolution of the local $dI(V,x)/dV$ spectra as a function of the distance x from the island edge measured in steps of 1 nm. Representative spectra are also shown in Fig. 2(d). The main spectral features are the following [see labels in Fig. 2(c)]: (A) Close to the interface, there is a proximity region where the spectra gradually evolve from one bulk behavior to the other over a distance of more than 100 nm. (B) A tiny yet important spectral feature is a small discontinuity in the height of the coherence peaks occurring at the S_1-S_2 interface on a subnanometer scale. (C,D) Far away from the island edge, the spectra go back to their bulk forms, S_1 (S_2), exhibiting a spatially constant superconducting gap Δ_1 (Δ_2). (E) Over about 60 nm from the S_1-S_2 interface, the spectra evolve in S_1 with slight changes toward the bulk S_1 spectrum, revealing the inverse proximity effect.

Before presenting how the tunneling conductance spectra are modified by increasing the temperature, it is convenient to first introduce the theoretical model that will help us to understand our observations. This is the goal of the next section.

III. THEORETICAL MODELING: USADEL EQUATIONS

Most theoretical studies of the proximity effect in S_1-S_2 systems have focused on the analysis of their critical

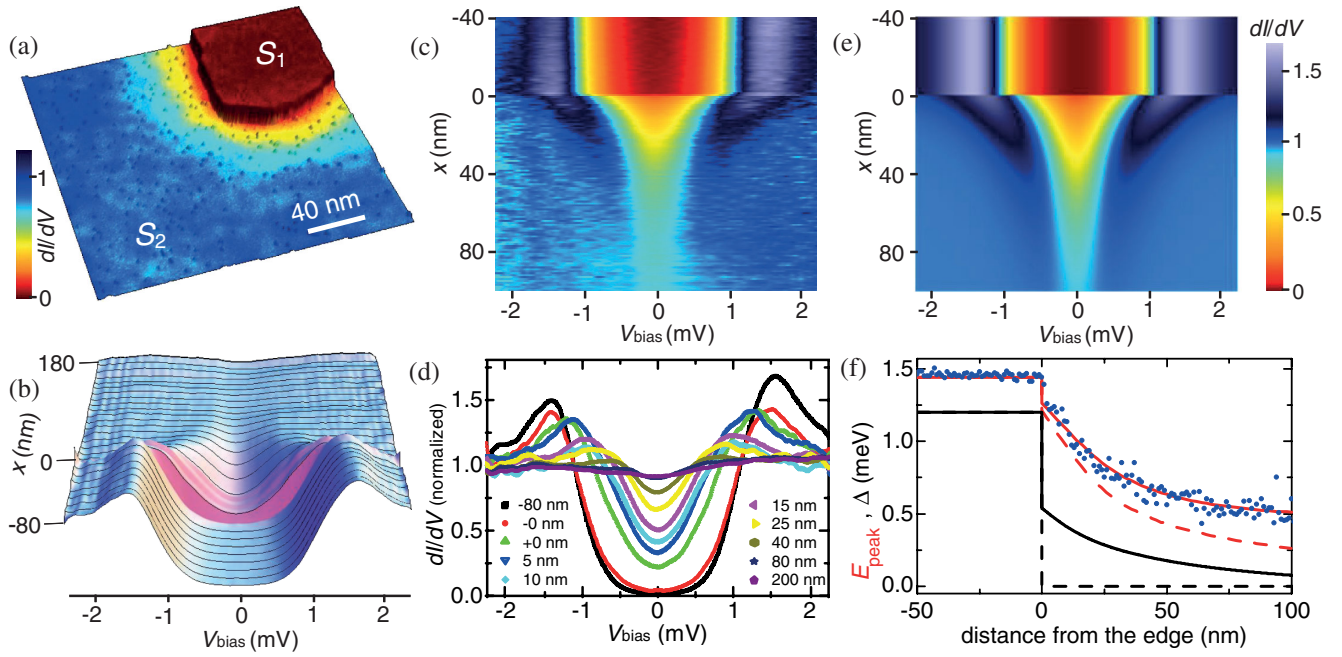

FIG. 3. The same as in Fig. 3, but for $T = 2.05$ K. At this temperature, the striped incommensurate Pb monolayer S_2 is in its normal state. Notice that the order parameter determined self-consistently exhibits a finite value close to the S_1-S_2 interface.

temperature. These studies have made use either of the Ginzburg-Landau theory or of the linearized Gorkov equations [2], which are only valid close to the critical temperature of the whole system [25]. Here, in order to describe the local spectra at arbitrary temperatures, we used the Usadel approach [26]. Usadel equations summarize the quasiclassical theory of superconductivity in the diffusive limit, where the mean free path is smaller than the superconducting coherence length. In the monolayer S_2, this length is given by $\xi_2 = \sqrt{\hbar D_2/\Delta_2}$. The quasiclassical theory describes all the equilibrium properties in terms of a momentum-averaged retarded Green's function $\hat{G}(\mathbf{R}, E)$, which depends on position $\mathbf{R}$ and energy E. This propagator is a 2×2 matrix in electron-hole space,

$$\hat{G} = \begin{pmatrix} g & f \\ \tilde{f} & \tilde{g} \end{pmatrix}. \tag{1}$$

Neglecting inelastic and phase-breaking interactions, the propagator $\hat{G}(\mathbf{R}, E)$ satisfies the following equation [26]:

$$\frac{\hbar D}{\pi}\nabla(\hat{G}\nabla\hat{G}) + [E\hat{\tau}_3 + \hat{\Delta}, \hat{G}] = 0. \tag{2}$$

Here, $\hat{\tau}_3$ is the Pauli matrix in electron-hole space and

$$\hat{\Delta} = \begin{pmatrix} 0 & \Delta(\mathbf{R}) \\ \Delta^*(\mathbf{R}) & 0 \end{pmatrix}, \tag{3}$$

where $\Delta(\mathbf{R})$ is the space-dependent order parameter that needs to be determined self-consistently via the following equation:

$$\Delta(\mathbf{R}) = \lambda \int_{-\epsilon_c}^{\epsilon_c} \frac{dE}{2\pi} \mathrm{Im}\{f(\mathbf{R}, E)\} \tanh\left(\frac{\beta E}{2}\right). \tag{4}$$

Here, $\beta = 1/k_B T$ is the inverse temperature, λ is the coupling constant, and ϵ_c is the cutoff energy. These two latter parameters are eliminated in favor of the critical temperature of the monolayer (in the absence of a proximity effect) in the usual manner. Moreover, in our case, with no phase difference between the superconducting reservoirs, the order parameter can be chosen to be real, as we have done implicitly in Eq. (4).

To solve the Usadel equations in practice, we modeled our lateral S_1-S_2 system by a one-dimensional (1 D) junction. Because of the big thickness difference between S_1 and S_2, we consider S_1 as an ideal reservoir in which the order parameter Δ_1 remains constant and unperturbed up to the interface (the observed tiny deviations due to the inverse proximity effect in S_1 are discussed below). S_2 is approximated as a semi-infinite wire with a constant attractive pairing interaction $\lambda(\mathbf{R}) = \lambda_2$ that corresponds to a critical temperature T_{C2}. Following Ref. [27], we solved the 1 D Usadel equations using the Ricatti parametrization [28] and described the junction interface with Nazarov's boundary conditions, valid for arbitrary transparency [29]. A key parameter in these boundary conditions is an effective reflectivity coefficient, r, roughly defined as the ratio between the resistances of the S_1-S_2 barrier and of the monolayer. Further technical details can be found in Appendix A. Within our 1 D model, we compute the local DOS $\rho(x, E)$ as a function of the distance to the interface, x, as $\rho(x, E) = -\mathrm{Im}\{g(x, E)\}/\pi$, while the corresponding normalized tunneling spectrum is given by

$$\frac{dI}{dV}(x,V) = -\int_{-\infty}^{\infty} dE\rho(x,E)\frac{\partial n_F(E-eV)}{\partial E}, \quad (5)$$

where $n_F(E)$ is the Fermi function.

Let us now use this model to describe the low-temperature results described in the previous section. For this purpose, we first fixed the bulk gaps in S_1 and S_2 by performing BCS fits of their local tunneling spectra acquired far away from the S_1-S_2 interface. The best fits were obtained for $\Delta_1 = 1.20$ meV and $\Delta_2 = 0.23$ meV, with an effective electron temperature of 0.55 K slightly higher than the base temperature of our STM (see Appendix B). Second, we determined the value of the effective reflectivity coefficient r by adjusting the discontinuity in the spectra observed at the interface. We obtained $r = 0.02$, which implies a highly transparent yet nonperfect interface. Third, we fixed the diffusion constant D_2 so as to reproduce the spatial dependence of the energy of the spectral maximum $E_{peak}(x > 0)$ [see Fig. 2(f)]. We obtained $D_2 \approx 7.3$ cm^2/s, which corresponds to a coherence length of $\xi_2 \approx 45.7$ nm, in nice agreement with the ξ_2 value extracted from the analysis of the vortex core profile in the striped incommensurate phase [21,30]. Moreover, the value of D_2 suggests that the mean free path is rather small (around 1 nm), and therefore, it is much smaller than ξ_2, which justifies the use of the Usadel approach.

Figure 2(f) shows that the theory captures the decay length of $E_{peak}(x)$, along with the observed jump at the island edge. In the same panel, we also show the self-consistent order parameter $\Delta(x)$ in the Pb monolayer: It exhibits a jump at the island edge and decays gradually to the S_2 bulk value within 80–100 nm. If the order parameter is not accounted for self-consistently, the calculated spatial dependence $E_{peak}(x)$ does not follow the experimental data [see dashed line in Fig. 2(f)]. This result emphasizes the need for a fully self-consistent calculation, which, in any case, is required based on fundamental principles. In Fig. 2(e), we show the $dI/dV(V,x)$ spectra obtained from the solution of the Usadel equations with the parameter values determined above. As one can see, the theory reproduces all the salient features of the experimental results of Figs. 2(c) and 2(d).

IV. GIANT PROXIMITY EFFECT: TEMPERATURES ABOVE T_{C2}

Let us now present and discuss the results for temperatures above the critical temperature of the monolayer. At $T = 2.05$ K, when S_2 is already in the normal state, the tunneling spectra change markedly [see Figs. 3(a) and 3(b)]. Now, the spectra in the Pb monolayer close to the interface exhibit a smooth induced gap that gradually disappears over a distance of around 60 nm away from the island edge. The overall evolution of the spectra resembles that recently reported by us in an S-N system, in which an amorphous Pb wetting layer played the role of a 2 D disordered normal metal [13]. However, there are two important differences with respect to the present case: (i) Here, the Altshuler-Aronov reduction of the low-bias tunneling density of states, characteristic of electronic correlations, is absent, and (ii) the crystalline monolayer is superconducting at lower temperatures while the disordered Pb wetting layer is not.

We now compare the proximity spectra with the results of our model using values of the parameters determined above, i.e., at 0.3 K. The effective temperature was taken to be equal to the bath temperature 2.05 K. The computed tunneling spectra are presented in Fig. 3(e). Again, the theoretical results qualitatively reproduce the experimental spectra of Fig. 3(c) with no adjustable parameters. More importantly, as we show in Fig. 3(f), the Pb monolayer locally develops, in the vicinity of the interface, a finite-order parameter that survives over a distance of more than 100 nm. The impact of this proximity-induced order parameter can be appreciated by comparing these results with a non-self-consistent calculation where the order parameter is assumed to vanish at this temperature, which would correspond to the situation where S_2 is a non-superconducting metal. Such a calculation shows that the induced gap extends over a much shorter distance inside the Pb monolayer as compared to the experimental dependence (see also Appendix C). This fact is illustrated in Fig. 3(f), where we show that the experimental data for $E_{peak}(x)$ are fitted much more satisfactorily by the self-consistent calculation. Thus, our results provide clear evidence for the existence of the proximity-induced superconductivity in the interface region. This phenomenon was already discussed theoretically by de Gennes and co-workers in the early 1960s [1], but to our knowledge, no direct observation has ever been reported. It is worth mentioning that the existence of this long-range or giant proximity effect has been suggested in the context of high-temperature superconductors based on the analysis of the supercurrent in trilayer Josephson junctions [31,32].

For completeness, we studied the proximity-induced interface superconductivity theoretically, in a more systematic manner. For this purpose, we computed the induced order parameter in S_2 for different temperatures (see Fig. 4). For temperatures below T_{C2}, the order parameter tends to a finite value far away from the island, while for higher temperatures, it asymptotically vanishes. Notice that right above T_{C2} (see the light green curve in Fig. 4), the induced order parameter can extend several hundreds of nanometers inside the monolayer. A detailed analysis of our numerical results in this temperature regime shows that away from the interface, the induced order parameter decays exponentially as $\Delta(x) \propto \exp(-x/L_\Delta)$, where L_Δ is a temperature-dependent decay length. As we illustrate in the inset of Fig. 4, this decay length diverges when T_{C2} is approached from above, approximately as $\sim 1/\sqrt{T - T_{C2}}$, which agrees with the prediction made with the help of the linearized

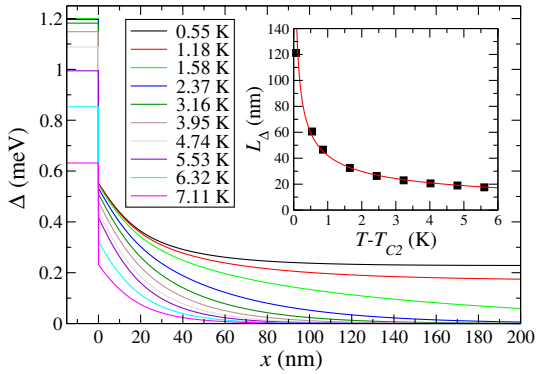

FIG. 4. The main panel shows the computed order parameter in the Pb monolayer as a function of the distance to the island edge for different temperatures. The critical temperature of the monolayer is, within BCS theory, $T_{C2} = 1.51$ K, while it is $T_{C1} = 7.89$ K for the island. The different parameters are those of Fig. 2(f), and the temperature dependence of Δ_1 has been taken into account. The inset shows the temperature dependence of the decay length L_Δ of the induced order parameter for temperatures above T_{C2} (see text for a definition). The symbols correspond to the values extracted from the curves shown in the main panel, while the red solid line is a numerical fit of those results to a function of around $1/\sqrt{T - T_{C2}}$.

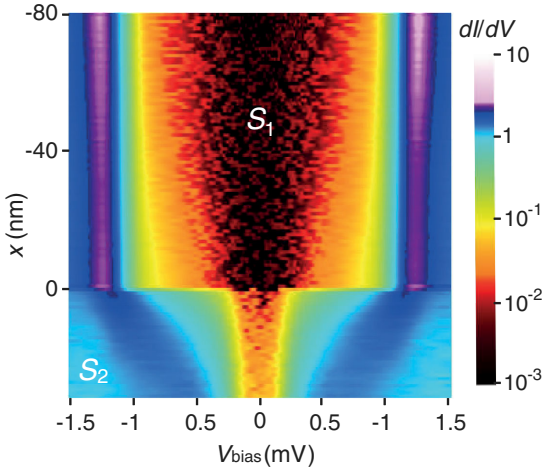

FIG. 5. Inverse proximity effect in the S_1 island at 0.3 K, and color-coded experimental $dI/dV(V, x)$ spectra across the S_1-S_2 junction. One spectrum is plotted every nanometer. The four-decade log color scale allows one to visualize two important effects as one approaches the S_1-S_2 interface: (i) reduction of the peak energy and amplitude (pink narrow $dI/dV > 1$ band) and (ii) appearance of a tail of induced subgap states in the region $\Delta_2 \leq eV_{\text{bias}} \leq \Delta_1$.

Gorkov equations [1,2]. It is worth stressing that at distances $x < L_\Delta$, the induced order parameter does not follow this simple exponential decay. On the other hand, notice also that when the temperature approaches T_{C1}, both the island's order parameter and the induced one in the monolayer vanish altogether. Thus, our analysis shows that the proximity effect in S_1-S_2 junctions is much richer than in the S-N case recently considered in Ref. [12].

V. DISCUSSION AND CONCLUSIONS

It is worth stressing that we also observed the so-called inverse proximity effect in the Pb island (see Fig. 5), which we ignored for simplicity in our calculations. Indeed, although the Pb island is much closer to being an electron reservoir than the atomically thin Pb monolayer, the electron density ratio between S_1 and S_2 is not infinite, and the superconductivity in S_1 is also affected near the interface by a contact to a weaker superconductor S_2. Nevertheless, the spectroscopic effects produced in S_1 are weak because of the large difference in electron densities of the two systems, and they require a four-decade log scale to be clearly visible. Figure 5 allows us to see two important features of the inverse proximity effect: (i) Following the coherence peak heights represented by the violet–light-pink bands (normalized conductance values above 1), one sees that the peak height slightly increases away from the S_1-S_2 interface while the energy of the peak maximum also slightly increases toward higher energy. (ii) Focusing now on the behavior of the low conductance values in the green-orange-brown region (10^{-3}-few 10^{-1}), a tail of induced subgap states appears in the excitation spectrum of S_1 in the energy window $|E| \in [\Delta_1, \Delta_2]$. This tail of induced states enables us to connect, by the edges, the large gap of S_1 to the small gap of S_2. In principle, the inverse proximity effect can be described within a natural extension of our 1 D model. However, as we discuss in Appendix D, such a description is not quite satisfactory, and this limitation calls for an extension of our model that is presently in progress.

To summarize, we have presented an experimental study of the proximity effect between two different superconductors, S_1 and S_2. Our system consists of an *in situ* fabricated lateral junction composed of a large-gap Pb island S_1 ($\Delta_1 = 1.20$ meV) and a small-gap crystalline atomic Pb monolayer S_2 ($\Delta_2 = 0.23$ meV). Making use of a low-temperature STM/STS, we have probed the local DOS of such a hybrid system with an unprecedented energy and space resolution. The observed proximity-induced modification of the tunneling spectra in the Pb monolayer S_2 was rationalized with the help of a 1 D model based on the self-consistent solution of the Usadel equations. In particular, our results show the appearance of proximity-induced interface superconductivity in S_2 in the vicinity of the S_1-S_2 interface for temperatures above T_{C2}, thus confirming the theoretical prediction by de Gennes and co-workers [1,2]. Our work not only elucidates this old-standing problem in the context of a proximity effect, but it also paves the way for studying new aspects of this quantum phenomenon such as the Meissner effect and vortex phases in proximity-induced superconductors. Finally, a weak inverse proximity effect is also revealed in the S_1 Pb island, characterized by both a slight reduction

of the coherence peak height and energy and by the appearance of a tail of induced subgap states. Further generalization of our 1 D model is needed to account for the inverse proximity effect.

ACKNOWLEDGMENTS

We thank Hugues Pothier, Cristian Urbina, and Guy Deutscher for useful discussions. V. C., C. B., T. C., F. D., V. S. S., and D. R. acknowledge various financial supports through the following French projects: the "Emergence" grant from the University Pierre et Marie Curie, the ANR grant Electrovortex. Financial support from the French-Russian project CNRS-PICS is also acknowledged. G. M. acknowledges funding from the CFM foundation providing its Ph.D grant. V. S. S. also acknowledges financial support from the Russian Foundation of Basic Research (RFBR) and from the Ministry of Education and Science of Russian Federation. J. C. C. acknowledges financial support from the Spanish MICINN (Contract No. FIS2011-28851-C02-01).

APPENDIX A: THEORETICAL DESCRIPTION OF THE PROXIMITY EFFECT—USADEL EQUATIONS

Our approach to describing the proximity effect is based on the Usadel equations [26]. The goal of this appendix is to provide some additional technical details about how they were solved in practice. In this discussion, we shall closely follow Ref. [27].

To describe the proximity effect in the crystalline monolayer, we modeled the Pb islands as ideal superconducting reservoirs and the monolayer as an infinite normal wire. To implement this model in practice, we considered a 1 D S_1-S_2'-S_2 junction, where S_1 and S_2 are BCS superconducting reservoirs with constant gaps $\Delta_{\text{island}} = \Delta_1$ and $\Delta_{\text{monolayer}} = \Delta_2$, respectively, and S_2' is a superconducting wire of the same material as the monolayer reservoir. The length of the central superconducting wire, L, was chosen sufficiently large as to avoid the influence of the presence of the S_2 reservoir in the density of states close to the interface with the S_1 reservoir. On the other hand, we neglected the inverse proximity effect in the S_1 reservoir (island), and we assumed that the S_2'-S_2 interface was perfectly transparent. However, we allowed the S_1-S_2' to be nonideal, as we explain in more detail below.

As explained in Sec. III, our technical task is to solve the Usadel equations [Eq. (2)], together with the corresponding equation for the order parameter [Eq. (4)]. Equation (2) must also be supplemented by the normalization condition $\hat{G}^2 = -\pi^2\hat{1}$. In order to numerically solve the Usadel equations, it is convenient to use the so-called Riccati parametrization [33], which automatically accounts for the normalization condition. In this case, the retarded Green's functions are parametrized in terms of two coherent functions, $\gamma(\mathbf{R}, E)$ and $\tilde{\gamma}(\mathbf{R}, E)$, as follows:

$$\hat{G} = -\frac{i\pi}{1+\gamma\tilde{\gamma}}\begin{pmatrix} 1-\gamma\tilde{\gamma} & 2\gamma \\ 2\tilde{\gamma} & \gamma\tilde{\gamma}-1 \end{pmatrix}. \tag{A1}$$

Using their definition in Eq. (A1) and the Usadel equation (2), one can obtain the following transport equations for these functions in the wire region [28]:

$$\partial_{\tilde{x}}^2\gamma + \frac{\tilde{f}}{i\pi}(\partial_{\tilde{x}}\gamma)^2 + 2i\left(\frac{E}{E_{\text{T}}}\right)\gamma = -i\frac{\Delta}{E_{\text{T}}}(1+\gamma^2), \tag{A2}$$

$$\partial_{\tilde{x}}^2\tilde{\gamma} + \frac{f}{i\pi}(\partial_{\tilde{x}}\tilde{\gamma})^2 + 2i\left(\frac{E}{E_{\text{T}}}\right)\tilde{\gamma} = i\frac{\Delta}{E_{\text{T}}}(1+\tilde{\gamma}^2), \tag{A3}$$

where we have used the fact that the order parameter is real. Here, $\tilde{x}$ is the dimensionless coordinate that describes the position along the S_2' wire, which ranges from 0 (S_1 lead) to 1 (S_2 lead), and $E_{\text{T}} = \hbar D_2/L^2$ is the Thouless energy of the wire. The expressions for $\tilde{f}$ and f are obtained by comparing Eq. (1) with Eq. (A1). Notice that Eqs. (A2) and (A3) couple the functions with and without tildes. However, for the system under study, one can show that the symmetry $\tilde{\gamma}(\mathbf{R}, E) = -\gamma(\mathbf{R}, E)$ holds, and therefore, only Eq. (A2) needs to be solved.

Now, we have to provide the boundary conditions for Eq. (A2). Since we want to describe a semi-infinite region of the striped incommensurate phase, we assume that the S_2'-S_2 interface is perfectly transparent. In this case, the boundary condition in this interface is simply given by the continuity of the coherent function:

$$\gamma(\tilde{x}=1, E) = \gamma_2(E) = -\frac{\Delta_2}{E^R + i\sqrt{\Delta_2^2 - (E^R)^2}}, \tag{A4}$$

with $E^R = E + i0^+$.

We allow the interface between the island and the monolayer wire to be nonideal, and to describe it, we used the boundary conditions derived in Refs. [29,34]. These conditions for a spin-conserving interface are expressed in terms of the Green's functions as follows:

$$\hat{G}_\beta\partial_{\tilde{x}}\hat{G}_\beta = \left(\frac{G_0}{G_{\text{N}}}\right)\sum_i \frac{2\pi^2\tau_i[\hat{G}_\beta, \hat{G}_\alpha]}{4\pi^2 - \tau_i(\{\hat{G}_\beta, \hat{G}_\alpha\} + 2\pi^2)}. \tag{A5}$$

Here, $\hat{G}_{\beta(\alpha)}$ refers to the Green's function on the monolayer (island) side of the interface, $G_0 = 2e^2/h$ is the quantum of conductance, and τ_i are the different transmission coefficients characterizing the interface. The parameter G_{N} is equal to $\sigma_2 S/L$, where σ_2 is the normal-state conductivity of the monolayer and S is the cross section of the barrier. Thus, G_{N} can be viewed as the normal-state conductance of a wire with cross section S and length L. In general, one would need the whole set $\{\tau_i\}$, but since one does not have access to this information, we adopt here a practical point of view. We assume that all the M interface open channels

have the same transmission τ, and we define $G_B = G_0 M\tau$ as the conductance of the barrier. Thus, the S_1-S_2' interface is characterized by two quantities, namely, the barrier conductance G_B and the transmission τ, and our starting point for the boundary conditions is

$$r\hat{G}_\beta \partial_{\tilde{x}} \hat{G}_\beta = \frac{2\pi^2[\hat{G}_\beta, \hat{G}_\alpha]}{4\pi^2 - \tau(\{\hat{G}_\beta, \hat{G}_\alpha\} + 2\pi^2)}, \tag{A6}$$

where we have defined the ratio $r = G_N/G_B$. In this language, an ideal interface is characterized by $r = 0$, and a tunnel contact is described by $\tau \ll 1$.

The next step is to express these boundary conditions directly in terms of the coherent functions. Substituting the definitions of Eq. (A1) into Eq. (A6), after straightforward algebra, one obtains the following boundary conditions for the coherent function γ at $\tilde{x} = 0$:

$$-r\frac{\partial_{\tilde{x}}\gamma_\beta - (\gamma_\beta)^2\partial_{\tilde{x}}\gamma_\beta}{(1-(\gamma_\beta)^2)^2} = \frac{(1+(\gamma_\beta)^2)\gamma_\alpha - (1+(\gamma_\alpha)^2)\gamma_\beta}{(1-(\gamma_\beta)^2)(1-(\gamma_\alpha)^2) + \tau(\gamma_\alpha - \gamma_\beta)^2}. \tag{A7}$$

This equation establishes a relation between the coherent function and its derivative evaluated on the side of the interface inside the S_2' wire (β) and the corresponding function evaluated on the side of the interface inside the S_1 reservoir (α), which is given by Eq. (A4) by replacing Δ_2 by Δ_1.

In summary, our main task was to solve Eq. (A2) together with Eq. (3) in a self-consistent manner. The nonlinear second-order differential equation of Eq. (A2), together with its boundary conditions in Eqs. (A4) and (A7), is a typical two-point boundary value problem. We solved it numerically using the so-called relaxation method, as described in Ref. [35]. On the other hand, the self-consistent loop was done using a simple iterative algorithm until convergence was achieved. Finally, the numerical solution for the coherent function was used to construct the retarded Green's function from Eq. (A1) and to compute the local density of states in the striped incommensurate phase region and the corresponding local tunneling conductance [see Eq. (5)].

APPENDIX B: BULK GAPS—BCS FITS

A first necessary step in the explanation of our experimental results is the determination of the zero-temperature bulk gaps of the island (Δ_1) and the Pb monolayer (Δ_2). For this purpose, we fitted the tunneling spectra measured at 0.3 K deep inside both superconductors with the bulk BCS theory, i.e., using the bulk BCS DOS in Eq. (5). To do the fits, we used both the zero-temperature gap and the temperature as adjustable parameters. The results of these fits are shown in Fig. 6. As one can see, the BCS theory satisfactorily reproduces the bulk spectra of both superconductors with an effective temperature of 0.55 K, which is slightly higher than the bath temperature of our experiments. The values obtained for the zero-temperature gaps are $\Delta_1 = 1.2$ meV and $\Delta_2 = 0.23$ meV. It is worth stressing that no artificial broadening was introduced in the expression of the BCS DOS to perform the fits.

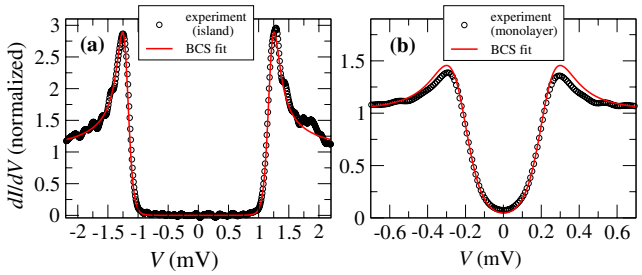

FIG. 6. Determination of the zero-temperature bulk gaps. (a) Normalized tunneling spectra as a function of the bias voltage. The symbols correspond to the experimental spectrum measured at 0.3 K deep inside the Pb island ($x = -80$ nm). The solid line corresponds to the best fit obtained with the BCS theory for $\Delta_1 = 1.2$ meV and $T = 0.55$ K. (b) The same as in the upper panel but for a spectrum measured in the Pb monolayer very far away from the island edge ($x = +200$ nm). The BCS tunneling spectrum was obtained using $\Delta_2 = 0.23$ meV and $T = 0.55$ K.

APPENDIX C: THEORETICAL RESULTS—REPRESENTATIVE EXAMPLES AND THE ROLE OF SELF-CONSISTENCY

We are not aware of any theoretical work on the proximity effect between two diffusive superconductors for arbitrary temperatures. For this reason, it may be of interest, for future reference, to provide here a more in-depth discussion of the results of the model described above.

In what follows, we fix the values of the zero-temperature gap of both superconductors to the values that best describe the experimental results, i.e., $\Delta_{\text{island}} = \Delta_1 = 1.2$ meV and $\Delta_{\text{monolayer}} = \Delta_2 = 0.23$ meV, corresponding to critical temperatures within the BCS theory equal to $T_{C1} = 7.89$ K and $T_{C2} = 1.51$ K. On the other hand, we also keep fixed the value of the diffusion constant in the crystalline monolayer to $D_2 = 7.3$ cm^2/s, which corresponds to a coherent length of $\xi_2 = 45.7$ nm. Let us start our analysis by considering the case in which the interface between the island and the monolayer is perfectly transparent ($r = 0$). Assuming a temperature of 0.55 K, which corresponds to the lowest effective temperature of the experiments, we have computed the local tunneling spectra in the monolayer as a function of the bias voltage for different positions along the monolayer, x, and the results can be seen in Fig. 7. Here, we show both the results obtained assuming a constant order parameter in the monolayer (see lower left panel), i.e., ignoring the self-

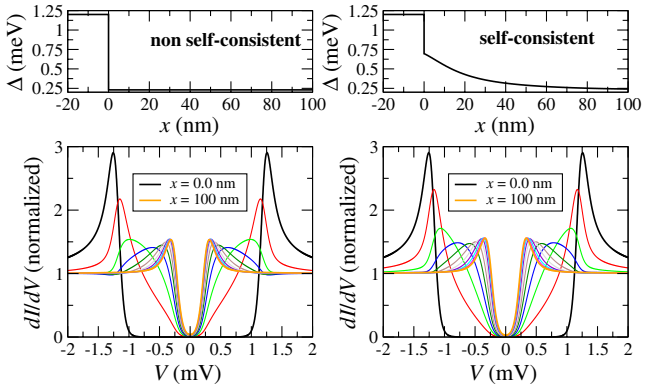

FIG. 7. The lower panels show the computed normalized dI/dV as a function of the bias voltage for $T = 0.55$ K and $r = 0.0$ (perfect transparency). The different curves correspond to different positions along the monolayer, x. The curves were computed in steps of 10 nm ranging from $x = 0$ (island edge) to $x = 100$ nm. The lower left panel corresponds to a calculation where the order parameter in the monolayer is assumed to be constant and equal to its bulk value. The lower right panel corresponds to the case in which the order parameter has been calculated in a self-consistent manner. The upper panels show the corresponding order-parameter profiles.

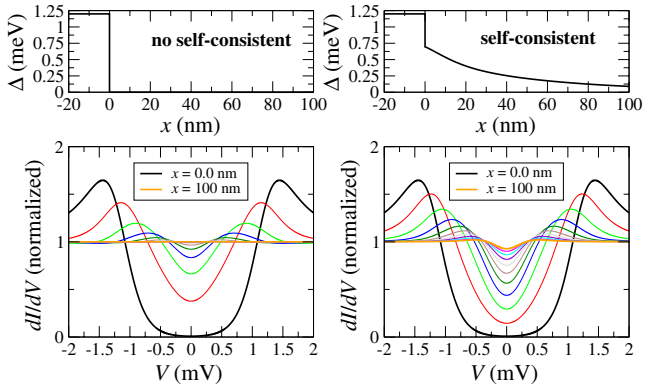

FIG. 8. The same as in Fig. 7, but for $T = 2.05$ K. At this temperature, the monolayer is in its normal state. Notice that the order parameter determined self-consistently exhibits a finite value in the vicinity of the island.

consistency, and the full self-consistent results (see lower right panel). We also show, in the upper panels, the corresponding profiles of the order parameter. The different curves in the lower panels correspond to different distances to the island edge ranging from 0 to 100 nm. The curves have been calculated in steps of 10 nm. As one can see, the spectra evolve gradually from the BCS-like spectrum at the island edge ($x = 0$ nm) for $\Delta = 1.2$ meV to the BCS-like spectrum deep inside the monolayer ($x = 100$ nm) for $\Delta = 0.23$ meV. In the vicinity of the island, the maximum of the spectra occurs in the range between the two bulk gaps (slightly shifted by the finite temperature), and it approaches Δ_2 at $\sim 2\xi_2$. Notice, however, that the spectra exhibit a space-independent gap equal to Δ_2. This result agrees with the results obtained by de Gennes using a variational method [1]. Notice also that the self-consistency increases the magnitude of the bias at which the spectra reach their maximum close to the interface, which is a consequence of the larger order parameter in that region.

Let us now consider a temperature of 2.05 K, which is above the critical temperature of the striped incommensurate monolayer. The corresponding results are shown in Fig. 8. In this case, one may naively expect the system to behave like an ordinary S-N system. However, this is not the case. As we show in the upper right panel of Fig. 8, the monolayer develops a finite order parameter close to the interface because of the proximity effect. This fact has a strong impact on the spectra. In particular, the induced gap that naturally appears in an S-N junction (see the non-self-consistent calculation in the lower left panel) now extends up to a much larger distance inside the monolayer, giving rise to a long-range proximity effect. As we have also discussed in Sec. IV (see Fig. 4), this phenomenon persists up to the critical temperature of the island, which, in this case, coincides with the critical temperature of the hybrid structure.

Irrespective of the temperature, in the previous results, the spectra evolve continuously from the island to the crystalline monolayer. This is a consequence of the assumed perfect transparency. However, the experimental results discussed in the main text show that there is a jump in the spectra when crossing the island edge. This suggests that the interface, although highly transparent, is not

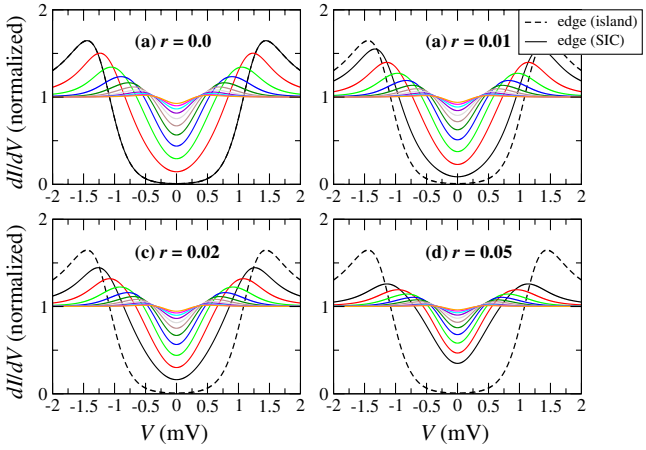

FIG. 9. Normalized tunneling conductance at $T = 0.55$ K as a function of the bias voltage for different values of the interface parameter r, as indicated in the panels. The different curves correspond to different positions along the monolayer, x. The curves were computed in steps of 10 nm ranging from $x = 0$ (island edge) to $x = 100$ nm. The black dashed lines in the different panels correspond to the spectra inside the island, while the black solid lines are the results obtained on the monolayer side of the island edge. Notice the discontinuity in the spectra at the island edge when $r \neq 0$.

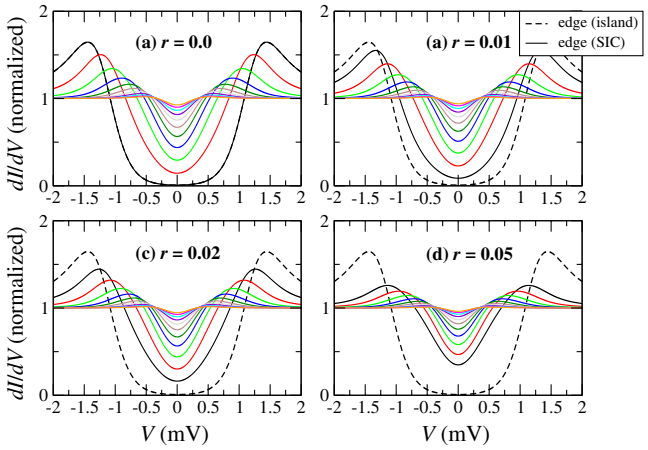

FIG. 10. The same as in Fig. 9, but for $T = 2.05$ K.

perfect. This discontinuity can be accounted for by using the boundary conditions described above. For simplicity, we assume that the transmission coefficient τ is equal to 1, and we attribute the nonideality of the interface to a non-negligible resistance of the barrier ($r \neq 0$). To illustrate the role of a finite value of the parameter r, we computed the tunneling spectra for different values of r for 0.55 and 2.05 K. The results are displayed in Figs. 9 and 10 and, as one can see, a finite r produces two main effects. First, a jump appears at the island edge, which increases in magnitude as r increases. Indeed, we have used the magnitude of this jump to adjust the value of r. Second, the peak's height in the spectra in the vicinity of the island

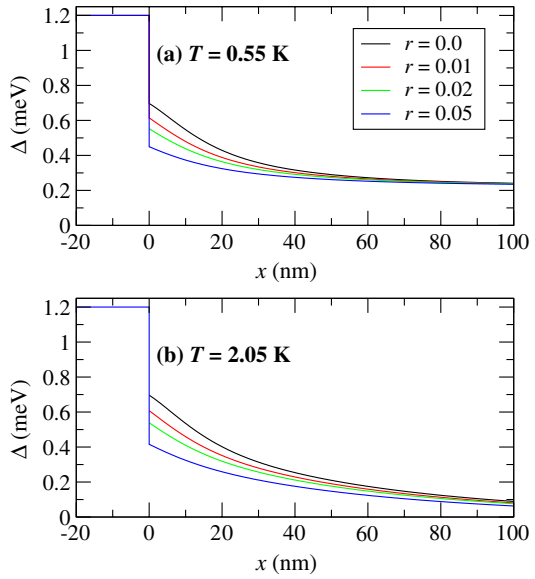

FIG. 11. Self-consistent order parameter as a function of the position for different values of r and for temperatures (a) $T = 0.55$ K and (b) $T = 2.05$ K. These profiles correspond to the cases shown in Figs. 9 and 10.

decreases as the value of r increases. If we keep increasing the value of r, the spectra in the monolayer would tend to be constant and we would recover the result for a bulk superconductor with its corresponding bulk gap (0.23 meV at 0.55 K and 0 meV at 2.05 K).

The finite interface resistance ($r \neq 0$) also has an obvious influence on the profiles of the order parameter. In Fig. 11, we show the order-parameter profiles corresponding to the different cases considered in Figs. 9 and 10. As one can see, a finite value of r reduces the amplitude of the order parameter in the vicinity of the island, thus reducing the proximity effect. Again, a very high value of r would simply kill the proximity effect in the monolayer.

A crucial point in our discussion is the marked difference between the self-consistent and non-self-consistent calculations, which is particularly clear for temperatures above

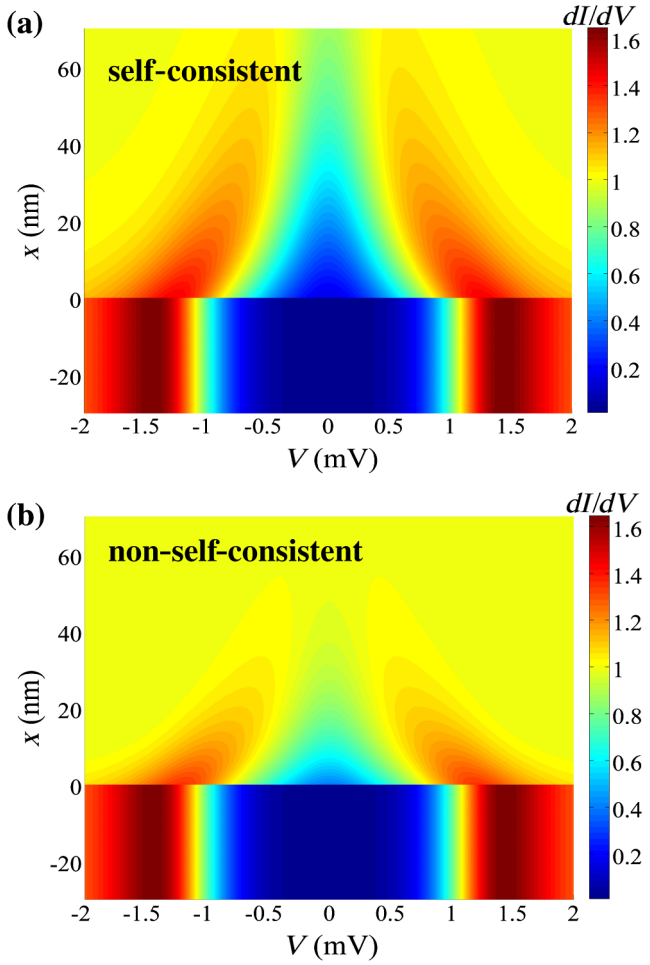

FIG. 12. Computed normalized tunneling spectra as a function of the bias and the position measured with respect to the island edge. (a) Results obtained in a self-consistent calculation using the following parameter values: $T = 2.05$ K, $\Delta_1 = 1.2$ meV, $\Delta_2 = 0.23$ meV, $r = 0.02$, and $D_2 = 7.3$ cm^2/s. (b) The same as in panel (a) but for a non-self-consistent calculation where the order parameter is assumed to vanish in the monolayer.

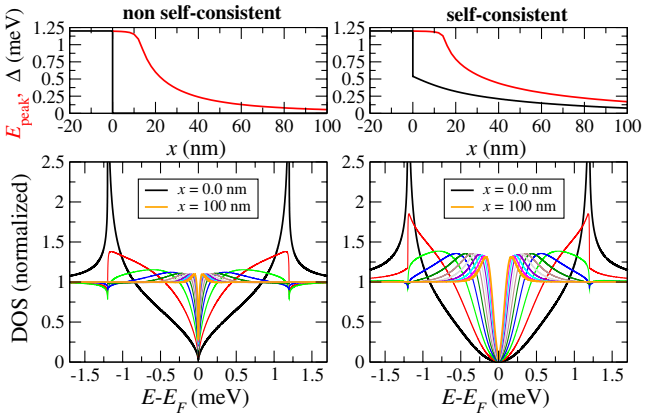

FIG. 13. The lower panels show the computed normalized density of states as a function of energy (measured with respect to the Fermi energy, E_F). The parameters of the model are those of Fig. 12, and the different curves correspond to different positions along the monolayer, x. The curves were computed in steps of 10 nm, ranging from $x = 0$ (monolayer side of the island edge) to $x = 100$ nm. The lower left panel corresponds to a calculation where the order parameter in the monolayer is assumed to be zero everywhere, while the lower right panel corresponds to the case in which the order parameter was calculated in a self-consistent manner. The upper panels show the corresponding order-parameter profiles (black lines) and the spatial evolution of the coherent peaks (red lines).

the critical temperature of the monolayer. This was already illustrated in Fig. 3(f), where we show that the experimental evolution of $E_{\mathrm{peak}}(x)$ at 2.05 K is much more satisfactorily described by the self-consistent result. For completeness, we show in Fig. 12 a comparison between the self-consistent and non-self-consistent calculations of the evolution of the tunneling spectra at 2.05 K in a 2 D plot for the same parameters as in Figs. 3(e) and 3(f). Notice that the color scale is different from the one used in the main text. As one can see, in the non-self-consistent case, the proximity effect extends a much smaller distance inside the monolayer. This is a natural consequence of the nonvanishing order parameter in the vicinity of the island that is found in the self-consistent calculation. This induced order parameter is reflected in a long-range proximity effect, as compared to the standard S-N case where N is a nonsuperconducting metal.

This long-range proximity effect can be better appreciated by looking directly at the local DOS, i.e., getting rid of the thermal broadening of the tunneling conductance. For this reason, in the lower panels of Fig. 13, we show a comparison of the spatial dependence of the local DOS for the cases shown in Fig. 12. We also include, in the upper panels, the corresponding profiles of the order parameter, as well as the evolution of the coherent peaks, defined as the position in energy of the maxima of the local DOS. As one can see in the lower panels, in both cases, the main feature in the local DOS is the appearance of an induced gap that progressively disappears as we move away from the interface—an induced gap that is obviously more pronounced than in the conductance spectra. In the non-self-consistent case, which corresponds to a standard S-N junction (with N being a nonsuperconducting metal), the decay of the induced gap away from the interface can be fitted by a function of the type $1/(1 + x/L_\xi)^2$, with $L_\xi = 14.3$ nm. This means that the induced gap roughly scales as a local Thouless energy $\hbar D_2/x^2$, as it is well known in standard diffusive S-N junctions [36]. In the self-consistent case, the decay of the induced gap can also be accurately described with the same type of function, but this time, the existence of a finite induced order parameter in the monolayer is manifested in a larger decay length, which we numerically found to be $L_\xi = 55.7$ nm for this example.

APPENDIX D: INVERSE PROXIMITY EFFECT

So far, we have assumed, in our theoretical analysis, that the island is a perfect reservoir with a constant order parameter. However, as discussed in Sec. V, our experiments show a small inverse proximity effect in the form of a reduction of the coherence peak amplitude and energy, as well as the appearance of subgap states in the excitation

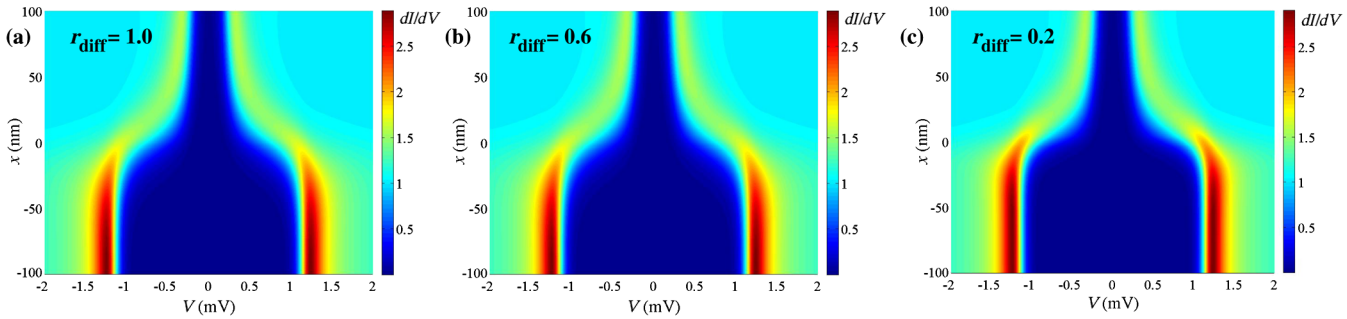

FIG. 14. Normalized tunneling spectra as a function of the bias voltage and the position measured with respect to the island edge. These results were obtained in self-consistent calculations that take into account the inverse proximity effect in the island. The three panels correspond to different values of the diffusion constant ratio $r_{\mathrm{diff}} = D_1/D_2$. The different parameter values are $T = 0.55$ K, $\Delta_1 = 1.2$ meV, $\Delta_2 = 0.23$ meV, $r = 0.0$, and $D_2 = 7.3$ cm^2/s.

spectrum of S_1 in the energy window $|E| \in [\Delta_1, \Delta_2]$. It is straightforward to extend the model discussed above to try to describe this inverse proximity effect. This simply requires solving the Usadel equation inside the island also, by taking into account that the pairing interaction constant λ takes different values in both electrodes, according to the corresponding critical temperatures. Moreover, we must consider that the diffusion constant can be different in both superconductors.

In Fig. 14, we present the results of the extension of our model to account for the inverse proximity effect. For simplicity, we have assumed a perfectly transparent interface, and the spatially resolved spectra are shown for different values of the ratio $r_{\mathrm{diff}} = D_1/D_2$, where D_1 and D_2 are the diffusion constants of the island and of the monolayer, respectively. As in the examples of the previous appendix, we have used the following parameter values: $T = 0.55$ K, $\Delta_1 = 1.2$ meV, $\Delta_2 = 0.23$ meV, and $D_2 = 7.3$ cm^2/s. These results suggest that the weak proximity effect observed inside the island could be naturally described within our model by simply assuming that D_1 is much smaller than D_2 (around 10 times smaller). However, given the small value of D_2, it seems unlikely that the Pb island could have such a small diffusion constant. We believe that this result might be an artifact of our 1 D model. A more natural explanation for the weak proximity effect would invoke the higher dimensionality of the island, which surely leads to a quick geometrical dilution of the order parameter inside. The confirmation of this idea would require performing 3 D simulations, which are out of the scope of this work. For this reason, and since the proximity effect inside the crystalline monolayer is indeed the main problem of interest in this work, in the main text we have decided to stick to the model in which the island is considered as a perfect superconducting reservoir.

[1] P. G. de Gennes, *Boundary Effects in Superconductors*, Rev. Mod. Phys. **36**, 225 (1964).

[2] G. Deutscher and P. G. de Gennes, *Superconductivity: Proximity Effects*, edited by R. D. Parks (Marcel Dekker, New York, 1969), Vol. 2, p. 1005.

[3] B. Pannetier and H. Courtois, *Andreev Reflection and Proximity Effect*, J. Low Temp. Phys. **118**, 599 (2000).

[4] A. F. Andreev, *Thermal Conductivity of the Intermediate State of Superconductors*, Sov. Phys. JETP **19**, 1228 (1964).

[5] S. Guéron, H. Pothier, N. O. Birge, D. Esteve, and M. H. Devoret, *Superconducting Proximity Effect Probed on a Mesoscopic Length Scale*, Phys. Rev. Lett. **77**, 3025 (1996).

[6] M. Meschke, J. T. Peltonen, J. K. Pekola, and F. Giazotto, *Tunnel Spectroscopy of a Proximity Josephson Junction*, Phys. Rev. B **84**, 214514 (2011).

[7] M. Vinet, C. Chapelier, and F. Lefloch, *Spatially Resolved Spectroscopy on Superconducting Proximity Nanostructures*, Phys. Rev. B **63**, 165420 (2001).

[8] N. Moussy, H. Courtois, and B. Pannetier, *Local Spectroscopy of a Proximity Superconductor at Very Low Temperature*, Europhys. Lett. **55**, 861 (2001).

[9] W. Escoffier, C. Chapelier, N. Hadacek, and J.-C. Villégier, *Anomalous Proximity Effect in an Inhomogeneous Disordered Superconductor*, Phys. Rev. Lett. **93**, 217005 (2004).

[10] H. le Sueur, P. Joyez, H. Pothier, C. Urbina, and D. Esteve, *Phase Controlled Superconducting Proximity Effect Probed by Tunneling Spectroscopy*, Phys. Rev. Lett. **100**, 197002 (2008).

[11] M. Wolz, C. Debuschewitz, W. Belzig, and E. Scheer, *Evidence for Attractive Pair Interaction in Diffusive Gold Films Deduced from Studies of the Superconducting Proximity Effect with Aluminum*, Phys. Rev. B **84**, 104516 (2011).

[12] J. Kim, V. Chua, G. A. Fiete, H. Nam, A. H. MacDonald, and C.-K. Shih, *Visualization of Geometric Influences on Proximity Effects in Heterogeneous Superconductor Thin Films*, Nat. Phys. **8**, 464 (2012).

[13] L. Serrier-Garcia, J. C. Cuevas, T. Cren, C. Brun, V. Cherkez, F. Debontridder, D. Fokin, F. S. Bergeret, and D. Roditchev, *Scanning Tunneling Spectroscopy Study of the Proximity Effect in a Disordered Two-Dimensional Metal*, Phys. Rev. Lett. **110**, 157003 (2013).

[14] C. Kumpf, O. Bunk, J. H. Zeysing, M. M. Nielsen, M. Nielsen, R. L. Johnson, and R. Feidenhans, *Structural Study of the Commensurate-Incommensurate Low-Temperature Phase Transition of Pb on Si(111)*, Surf. Sci. **448**, L213 (2000).

[15] L. Seehofer, G. Falkenberg, D. Daboul, and R. L. Johnson, *Structural Study of the Close-Packed Two-Dimensional Phases of Pb on Ge(111) and Si(111)*, Phys. Rev. B **51**, 13503 (1995).

[16] K. Horikoshi, X. Tong, T. Nagao, and S. Hasegawa, *Structural Phase Transitions of Pb-Adsorbed Si(111) Surfaces at Low Temperatures*, Phys. Rev. B **60**, 13287 (1999).

[17] D. Eom, S. Qin, M.-Y. Chou, and C. K. Shih, *Persistent Superconductivity in Ultrathin Pb Films: A Scanning Tunneling Spectroscopy Study*, Phys. Rev. Lett. **96**, 027005 (2006).

[18] T. Nishio, T. An1, A. Nomura, K. Miyachi, T. Eguchi, H. Sakata, S. Lin, N. Hayashi, N. Nakai, M. Machida, and Y. Hasegawa, *Superconducting Pb Island Nanostructures Studied by Scanning Tunneling Microscopy and Spectroscopy*, Phys. Rev. Lett. **101**, 167001 (2008).

[19] T. Cren, D. Fokin, F. Debontridder, V. Dubost, and D. Roditchev, *Ultimate Vortex Confinement Studied by Scanning Tunneling Spectroscopy*, Phys. Rev. Lett. **102**, 127005 (2009).

[20] C. Brun, I-Po Hong, F. Patthey, I. Yu. Sklyadneva, R. Heid, P. M. Echenique, K. P. Bohnen, E. V. Chulkov, and W.-D. Schneider, *Reduction of the Superconducting Gap of Ultrathin Pb Islands Grown on Si(111)*, Phys. Rev. Lett. **102**, 207002 (2009).

[21] T. Zhang, P. Cheng, W.-J. Li, Y.-J. Sun, G. Wang, X.-G. Zhu, K. He, L. Wang, X. Ma, X. Chen, Y. Wang, Y. Liu, H.-Q. Lin, J.-F. Jia, and Q.-K. Xue, *Superconductivity in One-Atomic-Layer Metal Films Grown on Si(111)*, Nat. Phys. **6**, 104 (2010).

[22] M. Yamada, T. Hirahara, and S. Hasegawa, *Magnetoresistance Measurements of a Superconducting Surface State of In-Induced and Pb-Induced Structures on Si(111)*, Phys. Rev. Lett. **110**, 237001 (2013).

[23] R. Feng, E. H. Conrada, M. C. Tringides, C. Kimb, and P. F. Miceli, *Wetting-Layer Transformation for Pb Nanocrystals Grown on Si(111)*, Appl. Phys. Lett. **85**, 3866 (2004).

[24] T. Cren, L. Serrier-Garcia, F. Debontridder, and D. Roditchev, *Vortex Fusion and Giant Vortex States in Confined Superconducting Condensates*, Phys. Rev. Lett. **107**, 097202 (2011).

[25] A notable exception is Ref. [11], where the authors used the Usadel equations to discuss the possibility of having an attractive pairing interaction in gold in the study of the proximity effect in an Al/Au bilayer.

[26] K. D. Usadel, *Generalized Diffusion Equation for Superconducting Alloys*, Phys. Rev. Lett. **25**, 507 (1970).

[27] J. C. Hammer, J. C. Cuevas, F. S. Bergeret, and W. Belzig, *Density of States and Supercurrent in Diffusive SNS Junctions: Role of Nonideal Interfaces and Spin-Flip Scattering*, Phys. Rev. B **76**, 064514 (2007).

[28] M. Eschrig, J. Kopu, A. Konstandin, J. C. Cuevas, M. Fogelström, and G. Schön, *Singlet-Triplet Mixing in Superconductor-Ferromagnet Hybrid Devices*, Adv. Solid State Phys. **44**, 533 (2004).

[29] Yu. V. Nazarov, *Novel Circuit Theory of Andreev Reflection*, Superlattices Microstruct. **25**, 1221 (1999).

[30] C. Brun *et al.* arXiv:1401.7876.

[31] I. Bozovic, G. Logvenov, M. A. J. Verhoeven, P. Caputo, E. Goldobin, and M. R. Beasle, *Giant Proximity Effect in Cuprate Superconductors*, Phys. Rev. Lett. **93**, 157002 (2004).

[32] L. Covaci and F. Marsiglio, *Proximity Effect and Josephson Current in Clean Strong/Weak/Strong Superconducting Trilayers*, Phys. Rev. B **73**, 014503 (2006).

[33] M. Eschrig, *Distribution Functions in Nonequilibrium Theory of Superconductivity and Andreev Spectroscopy in Unconventional Superconductors*, Phys. Rev. B **61**, 9061 (2000).

[34] J. Kopu, M. Eschrig, J. C. Cuevas, and M. Fogelström, *Transfer-Matrix Description of Heterostructures Involving Superconductors and Ferromagnets*, Phys. Rev. B **69**, 094501 (2004).

[35] W. H. Press, S. A. Teukolsky, W. T. Vetterling, and B. P. Flannery, *Numerical Recipes: The Art of Scientific Computing*, (Cambridge University Press, Cambridge, England, 1992).

[36] W. Belzig, C. Bruder, and G. Schön, *Local Density of States in a Dirty Normal Metal Connected to a Superconductor*, Phys. Rev. B **54**, 9443 (1996).